



Iron Metabolism, Pseudohypha Production, and Biofilm Formation through a Multicopper Oxidase in the Human-Pathogenic Fungus *Candida parapsilosis*

Tanmoy Chakraborty,^a Zsófia Tóth,^a Renáta Tóth,^a Csaba Vágvölgyi,^a  Attila Gácsér^{a,b}

^aDepartment of Microbiology, University of Szeged, Szeged, Hungary

^bMTA-SZTE Lendület Mycobiome Research Group, University of Szeged, Szeged, Hungary

ABSTRACT Among all the essential micronutrients, iron plays an important role in mammalian biology. It is also essential for pathogens infecting mammalian hosts, including bacteria, fungi, and protozoans. As the availability of accessible iron is limited within the mammalian host, several human-pathogenic fungal pathogens, such as *Candida albicans*, *Cryptococcus neoformans*, *Candida glabrata*, and *Aspergillus fumigatus*, have developed various iron uptake mechanisms. Although *Candida parapsilosis* is the second or third most common non-*albicans* *Candida* species associated with systemic and superficial *Candida* infections in immunocompromised patients, the mechanisms of iron uptake and homeostasis remain unknown in this fungus. In the current report, we show that a homologue of the multicopper oxidase gene *FET3* is present in the genome of *C. parapsilosis* (*CPAR2_603600*) and plays a significant role in iron acquisition. We found that homozygous deletion mutants of *CPAR2_603600* showed defects under low-iron conditions and were also sensitive to various stressors. Our results also revealed that the levels of pseudohypha formation and biofilm formation were reduced in the null mutants compared to the wild type. This phenotypic defect could be partially rescued by supplementation with excess iron in the growth medium. The expression levels of the orthologues of various iron metabolism-related genes were also altered in the mutants compared to the parental strain. In conclusion, our report describes the role of *CPAR2_603600* in iron homeostasis maintenance as well as morphology and biofilm formation regulation in this pathogenic fungus.

IMPORTANCE *C. parapsilosis* is the second or third most common opportunistic human-pathogenic *Candida* species, being responsible for severe fungal infections among immunocompromised patients, especially low-birth-weight infants (0 to 2 years of age). Among the major virulence factors that pathogenic fungi possess is the ability to compete with the host for essential micronutrients, including iron. Accessible iron is required for the maintenance of several metabolic processes. In order to obtain accessible iron from the host, pathogenic fungi have developed several iron acquisition and metabolic mechanisms. Although *C. parapsilosis* is a frequent cause of invasive candidiasis, little is known about what iron metabolic processes this fungus possesses that could contribute to the species' virulent behavior. In this study, we identified the multicopper oxidase *FET3* gene that regulates iron homeostasis maintenance and also plays important roles in the morphology of the fungus as well as in biofilm formation, two additional factors in fungal virulence.

KEYWORDS *Candida parapsilosis*, biofilms, fungal multicopper oxidase, pseudohypha

Iron is one of the most important micronutrients necessary for the growth and propagation of pathogens during an infection. It plays a crucial role in the structure of many proteins and in their enzymatic functions. Generally, it is incorporated into a

Citation Chakraborty T, Tóth Z, Tóth R, Vágvölgyi C, Gácsér A. 2020. Iron metabolism, pseudohypha production, and biofilm formation through a multicopper oxidase in the human-pathogenic fungus *Candida parapsilosis*. mSphere 5:e00227-20. <https://doi.org/10.1128/mSphere.00227-20>.

Editor Aaron P. Mitchell, University of Georgia

Copyright © 2020 Chakraborty et al. This is an open-access article distributed under the terms of the [Creative Commons Attribution 4.0 International license](https://creativecommons.org/licenses/by/4.0/).

Address correspondence to Attila Gácsér, gacsera@bio.u-szeged.hu.

Received 10 March 2020

Accepted 14 April 2020

Published 13 May 2020

heme complex or bound into iron sulfur clusters. Iron also acts as an important cofactor in different cellular processes such as the tricarboxylic acid (TCA) cycle, DNA replication, chromatin remodeling, mitochondrial respiration, and detoxification of reactive oxygen species (ROS) (1). Iron is a transition element which can exist in two oxidation states: a reduced ferrous (Fe^{2+}) form or a oxidized ferric (Fe^{3+}) form. The capacity of iron to gain or lose electrons is the reason why iron is the most important redox mediator in biology. Also, the divalent form of iron (Fe^{2+}) has the potential to catalyze the formation of cell-damaging hydroxyl radicals via the Fenton/Haber Weiss reaction (2).

In *Saccharomyces cerevisiae*, the Fet3 protein is required for high-affinity iron transport. The protein works downstream of the ferric reductases and is a cell surface ferroxidase belonging to the multicopper oxidase family (3). From expression analysis of *FET3*, it has been shown that it is regulated by the transcription factor Aft1p and the iron concentration of the environment. The mRNA transcripts of the genes *FRE1*, *FRE2*, and *FET3* are not detected in the absence of a functional *AFT1* gene (4). *FET3* mRNA levels were increased after growth in low-iron (1 to 10 μM) medium, whereas expression levels were below the detectable range when cells were grown in high-iron (1,000 μM) medium (5).

The crucial role of iron uptake and metabolism in human-pathogenic fungi such as *Candida albicans*, *Cryptococcus neoformans*, and *Aspergillus fumigatus* is well known, and the role of iron during opportunistic fungal infections has been extensively studied (6, 7). As *Candida* spp. belong to the normal human microbiota, various iron acquisition and metabolic mechanisms have evolved due to the hardships impeding accessible iron uptake. Pathways involved in *C. albicans* and *C. glabrata* iron metabolism have already been examined (8–11). Several genes have been revealed as necessary for reduction of ferric to ferrous iron and also for the uptake of reductive iron. The three main steps of reductive iron assimilation are (i) reduction of extracellular Fe^{3+} to Fe^{2+} , mediated by surface-bound ferric reductases; (ii) reoxidation of Fe^{2+} to Fe^{3+} by multicopper ferroxidases; and (iii) Fe^{3+} import by the permease Ftr1. Notably, *FET3* is required for the growth of *C. albicans* under iron-limiting conditions but not for virulence (12). Also, *C. albicans* has a transcription circuit for iron metabolism that enables survival within the human gastrointestinal tract as a commensal organism (13).

C. parapsilosis, a member of the CTG clade, is a major cause of neonatal candidiasis and also affects other patients with an immunocompromised status (14, 15). The hands of health care workers are often colonized by *C. parapsilosis*, which is the most relevant source of transmission and outbreaks in hospitals (16). There are various virulence factors that contribute to the pathogenicity of this species. These include adhesion to various biotic and abiotic surfaces, hydrolytic enzyme production, pseudohypha production, biofilm production on catheters and other implanted devices, eicosanoid production, and resistance to different classes of antifungal drugs (17). Although iron metabolism and its role in the virulence of the closely related species *C. albicans* have been well studied, little is known about iron homeostasis regulation and its relevance in the virulence of *C. parapsilosis*. Previously, it was reported that *CPAR2_100540*, a gene orthologous to *C. albicans* *HAP5* (*CaHAP5*), regulates iron metabolism as well as virulence in this species (18). Although *FET3* is not linked to virulence in *C. albicans*, we recently demonstrated that *C. parapsilosis* *FET3* (*CpFET3*), besides playing a role in prostaglandin production, influences its virulence (19); however, its role in iron metabolism remains unclear. In our current study, we showed that *CpFET3* is also involved in the regulation of iron metabolism and also influences fungal cell morphology and biofilm formation.

RESULTS

Identification of three multicopper oxidase genes in *C. parapsilosis* by *in silico* analysis and their expression under iron-limiting conditions. To identify multicopper oxidases in *C. parapsilosis*, a BLAST search was performed (www.candidagenome.org) (20) using *Saccharomyces cerevisiae* Fet3p (YMR058W) as the query sequence. We identified only three genes in the multicopper oxidase family with >40% identity to the

query sequence, which is in contrast with the identification of the five *FET3* orthologs *FET3*, *FET31*, *FET33*, *FET34*, and *FET99* in analyses of *C. albicans* (see Fig. S2 in the supplemental material) (8). The three genes identified were *CPAR2_603600*, *CPAR2_304050*, and *CPAR2_603590* (Fig. S1). The results of multiple-sequence alignment (21, 22) showed that *CPAR2_603600p*, *CPAR2_603590p*, and *CPAR2_304050p* have 79%, 75.3%, and 66% sequence identity with *CaFet3p*, *CaFet99p*, and *CaFet33p*, respectively (Fig. S3). To examine if these genes might be associated with iron metabolic processes, we assessed their expression levels under iron-limited conditions using three different *C. parapsilosis* isolates: CLIB214, CBS1954 (23), and CDC17. For growth, 100 μM /ml bathophenanthroline disulfonate (BPS)-supplemented YPD (1% dextrose, 1% peptone, and 0.5% yeast extract) liquid medium was used. As a control, cells were also grown without the addition of BPS. According to our results, the expression of *CPAR2_603600* was significantly elevated in all three isolates compared to that of the other two genes, suggesting its greater influence under iron-limited growth conditions (Fig. 1A).

***CPAR2_603600* regulates growth under low-iron conditions.** To thoroughly investigate the role of *CPAR2_603600* in iron metabolism, two independent homozygous deletion mutants (the $\Delta/\Delta603600$ 1/1 and $\Delta/\Delta603600$ 2/1 mutants) were generated using *C. parapsilosis* isolate CLIB214 as a parental strain. Gene deletion was performed using the fusion PCR-based auxotrophy complementation method previously described by Holland et al. (24). For all the subsequent analyses, a *CPAR2_603600* reintegrant (RI) mutant strain was also applied. To examine the effect of gene deletion on growth under conditions of iron starvation, parental, reintegrant, and null mutant strains were spotted on YPD plates supplemented with 50, 100, and 150 $\mu\text{g}/\text{ml}$ BPS, chelating ferrous iron (II). Nonsupplemented YPD medium was also used as a control. Although all analyzed strains grew similarly on YPD plates, the $\Delta/\Delta603600$ 1/1 and $\Delta/\Delta603600$ 2/1 strains showed a remarkable growth deficiency under iron-limited conditions (>100 $\mu\text{g}/\text{ml}$ BPS) compared to the wild-type (WT) strain and the RI strains, suggesting that *CPAR2_603600* is required for viability only under low-iron conditions (Fig. 1B). We also analyzed the expression of *CPAR2_304050* and *CPAR2_603590* in the absence of *CPAR2_603600*. As shown in Fig. 1C, expression of *CPAR2_603590* increased remarkably in the deletion mutant strain compared to the parental strain but that of *CPAR2_304050* did not (Fig. 1A), suggesting a potential compensatory effect in the case of *CPAR2_603590*.

The $\Delta/\Delta603600$ mutant showed growth defects under stress-inducing conditions. Phenotypic characterization of the deletion mutants was performed by growth analyses under 19 different growth conditions, including different temperatures, different pH levels, and the presence or absence of cell wall stressors, cell membrane stressors, osmotic stressors, oxidative stressors, and heavy-metal stressors (Fig. 2). The mutants showed a growth-deficient phenotype at lower temperature (25°C) and alkaline pH in the presence of the cell wall stressor Congo red, a cell membrane stressor (SDS), an oxidative stressor (menadione), and a heavy-metal stressor (cadmium sulfate), whereas the mutants were less sensitive to heavy-metal copper. There were no differences in the levels of growth in the presence of osmotic stress created by sorbitol or glycerol, although null mutant strains showed a slight growth defect in response to NaCl.

***CPAR2_603600* influences morphology transition.** One of the most important virulence traits of *C. parapsilosis* is its ability to produce pseudohyphae. In *C. albicans*, two iron metabolism regulatory genes, *TUP1* and *FET34*, regulate filamentous growth (25, 26). Thus, we examined whether *CPAR2_603600* has a similar effect in *C. parapsilosis*. Interestingly, deletion of *CPAR2_603600* resulted in a significant reduction in pseudohypha formation both on solid medium and in liquid medium compared to the wild-type strain and the reintegrant strains (Fig. 3). A difference in colony wrinkling between the wild-type strain and the mutant strains was detected on solid Spider medium after 7 days of incubation at 37°C (Fig. 3A). Microscopic pictures of the colony edges on Spider medium revealed similar differences and thus reduced pseudohypha

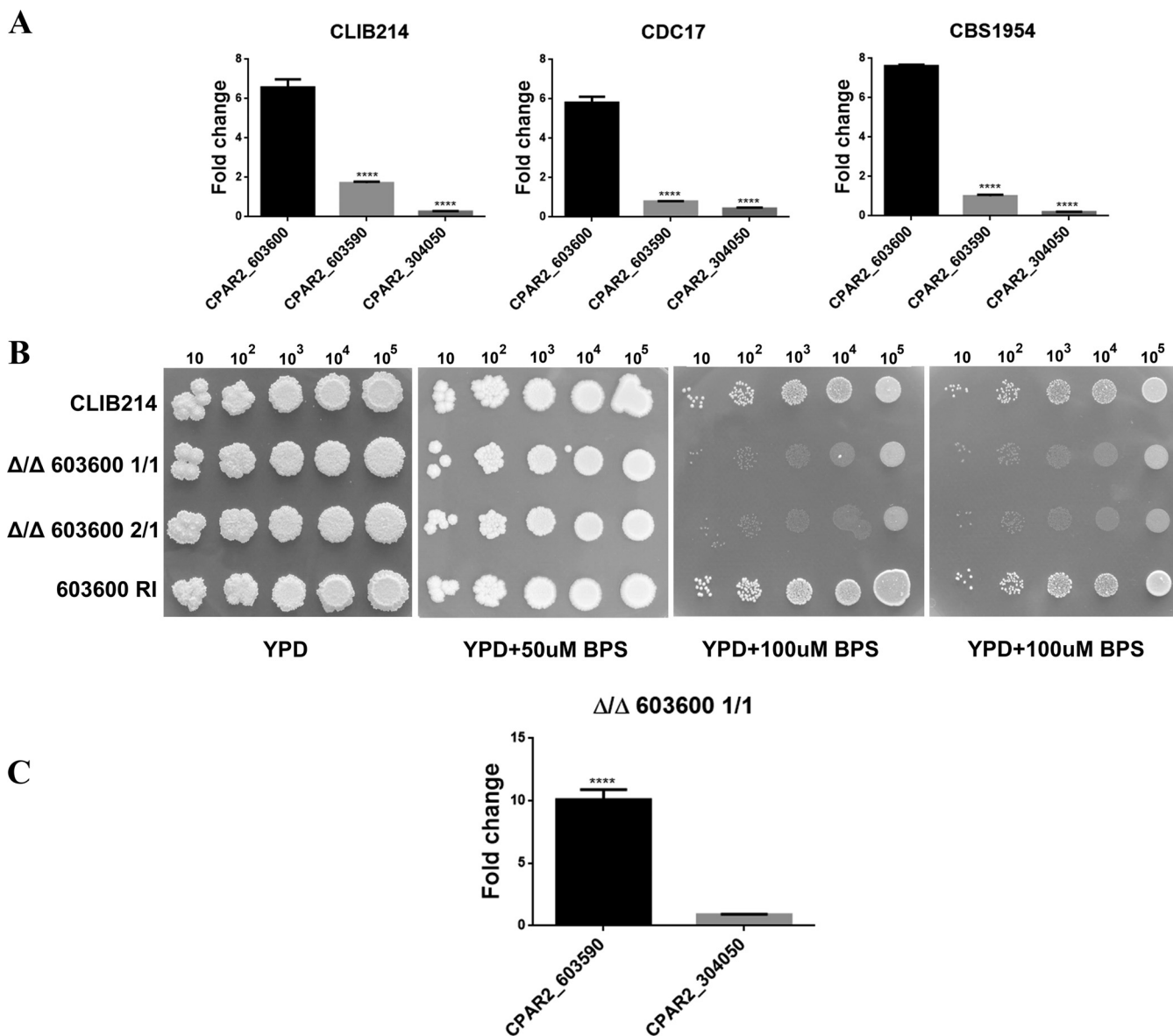


FIG 1 Expression analysis of multicopper oxidase-encoding genes and the effect of *CPAR2_603600* deletion on growth. (A) Expression analysis of *CPAR2_603600*, *CPAR2_304050*, and *CPAR2_603590* in CLIB 214, CDC17, and CBS1954 *C. parapsilosis* isolates under low-iron conditions. Fold change expression was calculated taking YPD growth as the control condition. Statistical significance was calculated using one-way ANOVA coupled with Dunnett's *post hoc* test (****, $P \leq 0.0001$). (B) Growth analysis of CLIB 214 parental, $\Delta/\Delta 603600$ 1/1, $\Delta/\Delta 603600$ 2/1, and *603600 RI* strains in the absence and presence of the iron chelator BPS in increasing concentrations. Images were taken after 3 days of incubation at 30°C. (C) Expression of *CPAR2_603590* and *CPAR2_304050* in the absence of *CPAR2_603600*. Statistical significance was calculated using the test mentioned above (****, $P \leq 0.0001$).

formation of the $\Delta/\Delta 603600$ 1/1 mutant compared to the parental strain (Fig. 3B). Single-colony analysis of the wild-type strain and the $\Delta/\Delta 603600$ 1/1 strain on Spider medium also showed a difference in colony morphology (Fig. S4). Quantitative analysis of pseudohypha formation was also performed using liquid medium (Fig. 4). In liquid Spider medium, pseudohypha formation was enhanced (for the wild-type strain, 9.41% in YPD control medium versus 17.7% in Spider medium). Furthermore, under the same condition, the $\Delta/\Delta 603600$ 1/1 mutant strain showed a significant reduction in pseudohypha formation (3.26%) compared to the wild-type strain (17.7%). Scanning electron microscopy (SEM) images of wild-type and $\Delta/\Delta 603600$ 1/1 cells further supported the data indicating a decreased amount of pseudohyphae present in the mutant strain (Fig. 5).

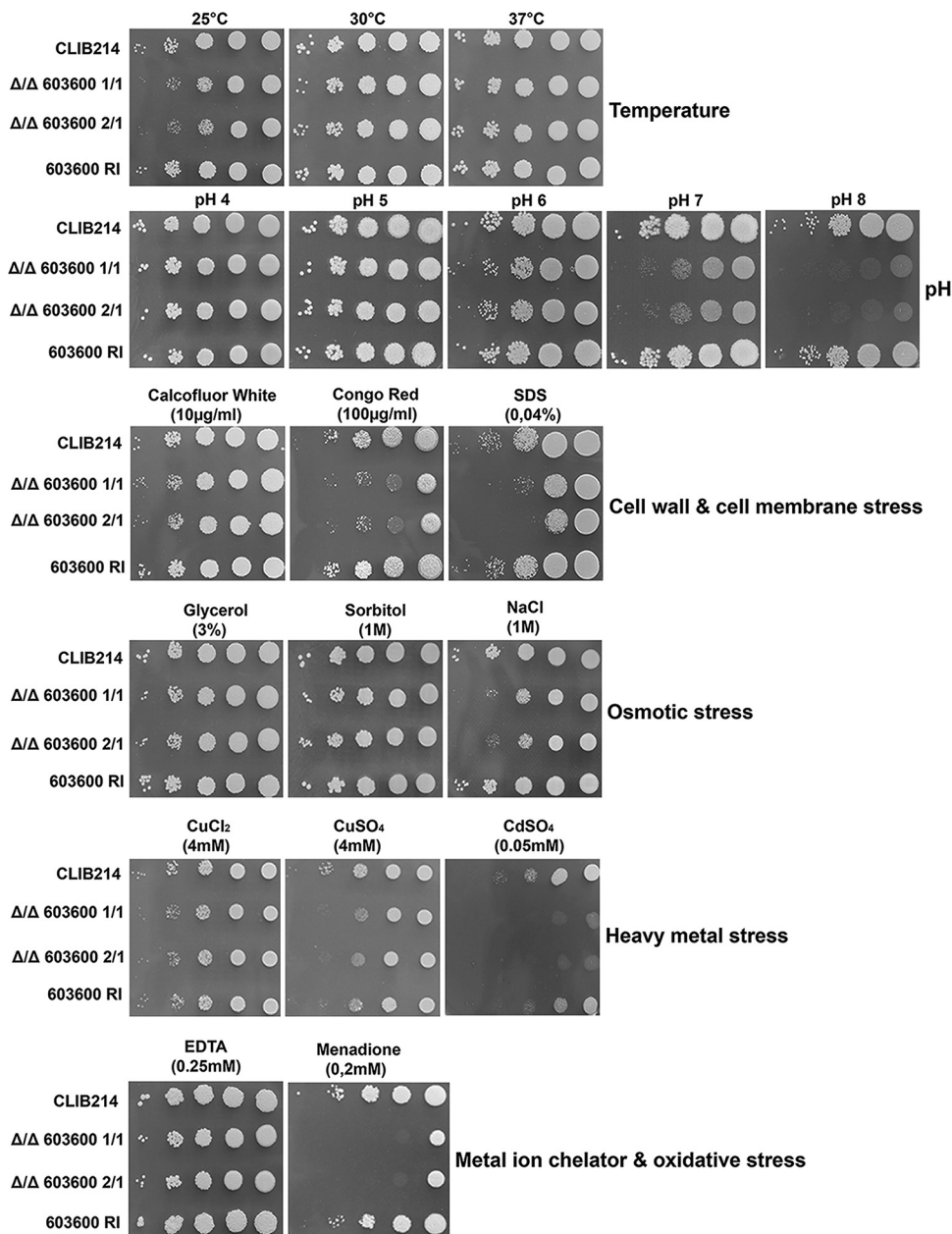


FIG 2 Phenotypic characterization of the mutant under different growth conditions. Results of phenotypic screening of the CLIB parental strain, $\Delta/\Delta 603600$ homozygous deletion mutants, and the *603600 RI* strain under various growth conditions, including different temperatures and pH levels and YPD medium supplemented with osmotic stressors, cell wall stressors, cell membrane stressors, oxidative stressors, or heavy-metal stressors, are shown. Different dilutions of cells were spotted on each plate, and pictures were taken after 2 days of growth at 30°C.

Deletion of *CPAR2_603600* decreased biofilm formation. Another major *C. parapsilosis* virulence factor is the ability to form biofilms on abiotic surfaces such as medical implants. Mature *C. parapsilosis* biofilms consist of both pseudohyphae and yeast cells. Reductions in the amount of pseudohyphae prompted us to examine if *CPAR2_603600* also affects biofilm formation in this species. Biofilm formation of the wild-type, null mutant, and reintegrant strains was measured using the 2,3-bis-(2-methoxy-4-nitro-5-sulfophenyl)-2H-tetrazolium-5-carboxanilide salt (XTT) metabolic assay. According to our results, the null mutant strains showed a significant decrease in biofilm formation compared to the parental and reintegrant strains (Fig. 6), suggesting that the role of *CPAR2_603600* is not restricted to iron metabolism and filamentous growth regulation.

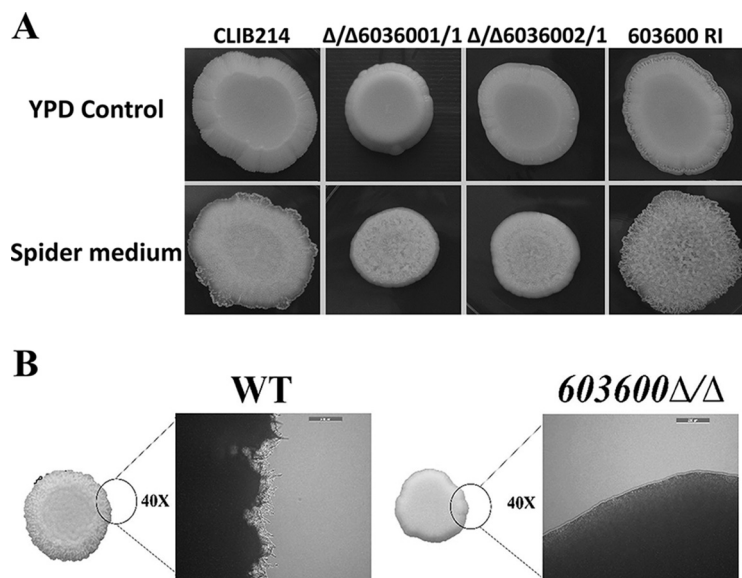


FIG 3 Decrease in pseudohypha formation in the absence of *CPAR2_603600*. (A) Colony morphology of the *CPAR2_603600* mutant and wild-type strains was analyzed in pseudohypha-inducing medium (Spider medium) maintained at 37°C after 7 days. The YPD plate served as a control. (B) Microscopic images of the edge of wild-type (WT) and $\Delta/\Delta603600$ 1/1 colonies on solid Spider medium (scale bar, 160 μm).

Supplementation with additional iron rescued the defective phenotypes of $\Delta/\Delta603600$ mutants. To examine if the defects in pseudohypha and biofilm formation could be rescued by the reintroduction of iron into the growth medium, all strains were grown in YPD supplemented with 2 mM FeCl_3 overnight at 30°C, prior to the follow-up examinations. Pseudohypha formation and biofilm formation were examined using methods similar to those described above. Our results revealed that the $\Delta/\Delta603600$ mutant cells regained their ability to form pseudohyphae similarly to the wild-type and reintegrant strains based on colony morphology (Fig. 7). XTT metabolic experiments revealed a partial rescue of the biofilm defect of $\Delta/\Delta603600$ cells by iron supplementation (Fig. 8). Together, these results suggest that supplementation with accessible iron at least partially restores the defective phenotypes gained by *CPAR2_603600* deletion.

Expression of genes related to iron metabolism in the deletion mutant strains.

Next, we examined if the lack of *CPAR2_603600* alters the expression of other genes related to iron metabolism. We selected 14 genes (Table 1) by GO term analysis from the *Candida* genome database, based on their orthologues regulating iron homeostasis in *C. albicans*. Using quantitative reverse transcription-PCR (qRT-PCR) analysis, we found that 9 of the 14 analyzed genes showed an increase in expression (average fold change, ≥ 2) in the $\Delta/\Delta603600$ 1/1 mutant strain compared to the normalized wild-type values (WT value = 1). Those 9 genes included *RBT5*, *HAP43*, *FTH1*, *FTR1*, *SIT1*, *HMX1*, *SEF1*, *CFL5*, and *CCC2* (Fig. 9). Thus, in the absence of *CPAR2_603600*, altered expression of genes corresponding to ferric reductase, ferrous iron transport, and ferrous iron permease was detected, indicating the presence of a potential compensatory effect.

Altered expression of hypha and biofilm regulatory genes in the deletion mutant strain. We next analyzed the expression of genes related to biofilm formation and pseudohypha regulation in *C. parapsilosis*, namely, *EFG1*, *UME6*, *CPH2*, *GZF3*, *BCR1*, *ACE2*, and *CZF1*. Prior to RNA isolation, the wild-type strain and the deletion mutant strain were grown in the filamentous-growth-inducing Spider medium at 37°C (Fig. 10A) and in YPD medium at 30°C (Fig. 10B). Quantitative PCR (qPCR) analysis revealed that even under noninducing conditions, 4 of the 7 examined genes showed a mild decrease in expression relative to the wild-type strain (Fig. 10B). Under filamentous-growth-inducing conditions, all examined pseudohypha and biofilm reg-

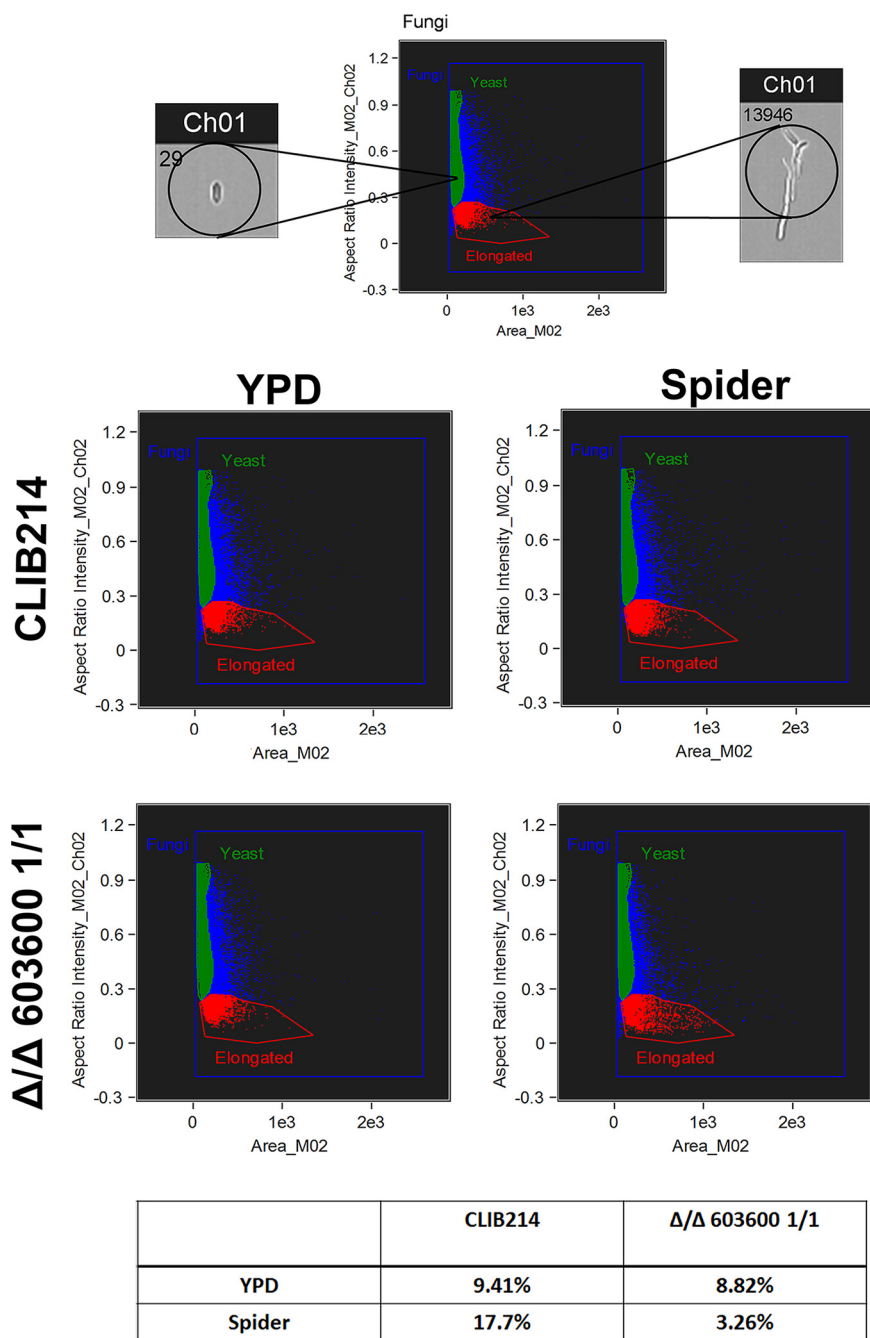


FIG 4 Percentage of pseudohypha formation by FACS analysis. Pseudohypha formation was determined by quantitative FACS analysis after growth in YPD and pseudohypha-inducing media at 37°C in the presence of 5% CO₂.

ulatory genes were markedly downregulated relative to the corresponding genes' normalized values (set to 1) in the wild-type strain (Fig. 10A).

Deletion of *CPAR2_603600* in an environmental isolate of *C. parapsilosis*. To examine if *CPAR2_603600* plays a similar role in other *C. parapsilosis* isolates, a homozygous deletion mutant strain was also generated in the CBS1954 environmental isolate (23) using the SAT1 flipper cassette method (27). We found that the CBS1954 ΔΔ*M20/1* deletion mutant showed a similar growth defect in the absence of accessible iron (see "YPD +BPS" data in Fig. 11A) and defects in pseudohypha formation (Fig. 11C) as well as in biofilm formation (Fig. 11D). In the generated null mutant strain, the expression

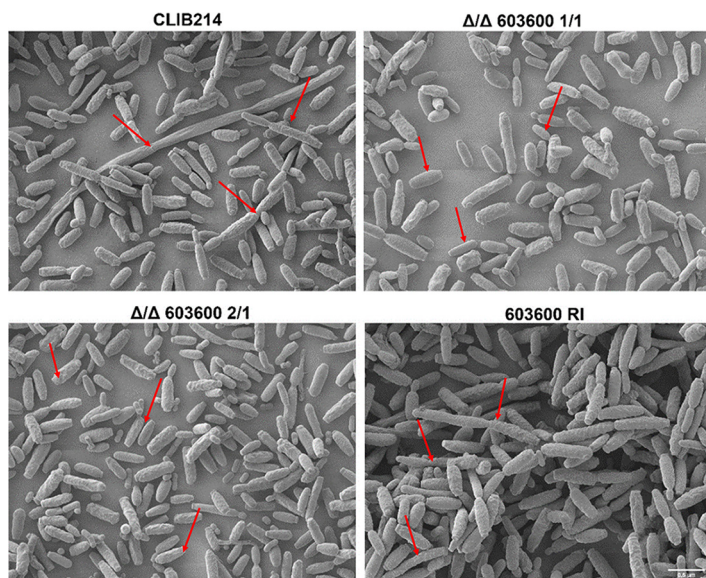


FIG 5 Scanning electron microscopic images of the wild-type and *CPAR2_603600* mutant strains. All strains were visualized using SEM after growth in Spider medium at 37°C for 24 h. Arrows indicate greater numbers of elongated pseudohyphal cells in wild-type and reintegrant strains than in the null mutants, where most of the yeast cells were smaller.

levels of both *CPAR2_603590* and *CPAR2_304050* were higher than the level seen in the parental strain (Fig. 11B). Similarly to the $\Delta/\Delta603600$ 1/1 mutant results, the expression levels of several of the 14 iron metabolism regulatory genes examined were also increased in the *CBS1954* $\Delta/\Delta M20/1$ strain (average fold change, ≥ 2) compared to the normalized wild-type values (*CBS1954* or WT = 1) (Fig. 11E). Furthermore, qPCR analysis also revealed that biofilm and pseudohypha regulatory genes were downregulated both under noninducing conditions and under filamentous-growth-inducing conditions relative to the corresponding genes' normalized values in the wild-type strain, similarly to what was observed in $\Delta/\Delta603600$ 1/1 (Fig. 11F and G). These observations confirmed that the effect of *CPAR2_603600* gene deletion is strain independent.

DISCUSSION

Among all the metals, iron plays one of the most important roles in fungal pathogenesis. The availability of free iron is restricted in the blood by the host to

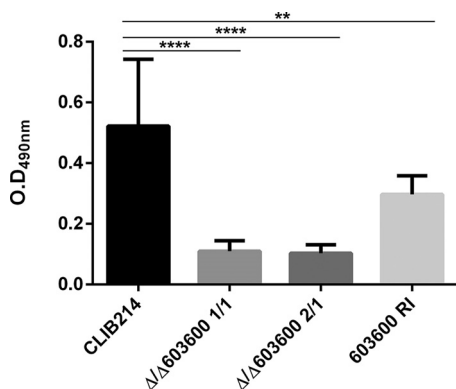


FIG 6 Loss of *CPAR2_603600* results in decreased biofilm formation. The CLIB 214 wild-type, deletion mutant, and reintegrant strains were grown in Spider medium at 37°C for 48 h, and biofilm formation was determined using the XTT cell viability assay. Three independent experiments were performed for biofilm analysis by XTT assay. One-way ANOVA with Dunnett's *post hoc* test was used to determine statistical significance (**, $P \leq 0.01$; ****, $P \leq 0.0001$).

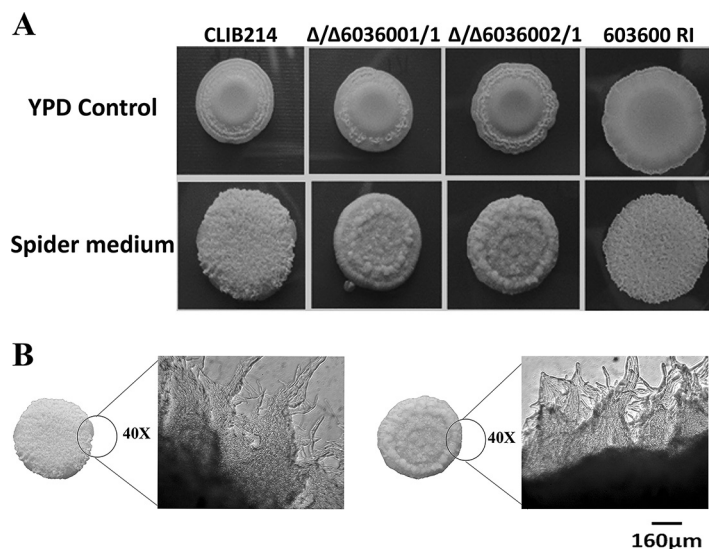


FIG 7 Morphology defect rescued by addition of iron to the preculturing medium. (A) Pseudohypha production was analyzed after growth of each strain overnight at 30°C in 2 mM FeCl_3 -supplemented YPD as a preculturing medium. Cells were then plated on pseudohypha-inducing medium, and images were taken after 7 days of incubation at 37°C. Addition of excess iron to the preculturing medium (YPD) rescued the defective phenotype on solid plates. (B) Microscopic images of the edge of wild-type and $\Delta/\Delta 603600$ 1/1 colonies on solid Spider medium (scale bar, 160 μm).

provide nutritional immunity. Analyses of the role of metal homeostasis in virulence of human-pathogenic fungi such as *C. albicans*, *C. neoformans*, and *A. fumigatus* have been reported from numerous previous studies (7). *Candida* spp., being commensal pathogens, evolved different iron uptake mechanisms to survive within different host niches (28). *C. albicans* utilizes different iron sources from the host through siderophores of other microorganisms or via hemoglobin, transferrin, lactoferrin, and ferritin present within the host. The main pathways involved in iron homeostasis in *C. albicans* include surface ferric reductases (*CFL1* and *FRE1* [29] and *CFL95*, *FRE10*, and *RBT2* [29, 30]), multicopper oxidases (*FET3* and *FET99* [12, 31]), and high-affinity iron permeases (*FTR1* [32]). Among the five multicopper oxidase genes present in *C. albicans*, a mutant with a deletion of the *FET3* gene showed a growth defect under low-iron conditions and a reduction in prostaglandin production (33); however, it remained as virulent as the wild-type strain. Deletion of *FET34* resulted in a slight growth defect under

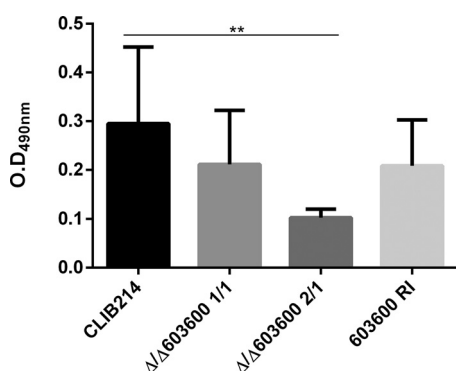


FIG 8 Addition of excess iron to the preculture medium partially rescued the biofilm defect of the deletion mutants. Addition of 2 mM FeCl_3 to the YPD preculture medium partially rescued the biofilm formation defect. After preculturing of all strains in iron-supplemented YPD, cells were transferred to liquid Spider medium and incubated at 37°C. After 48 h, the XTT assay was applied to measure potential alterations in biofilm formation. Two independent experiments were performed for the biofilm assay. One-way ANOVA with Dunnett's *post hoc* test was used to determine statistical significance (**, $P \leq 0.05$).

TABLE 1 List of genes related to iron metabolism in *C. parapsilosis* with their corresponding homologue in *C. albicans*

CPAR gene ID ^a	<i>Candida albicans</i> homologue	Function
CPAR2_210110	<i>CFL5</i>	Ferric reductase; induced low iron; ciclopirox olamine, flucytosine induced; amphotericin B, Sfu1 repressed; Tbf1, Hap43 induced
CPAR2_700570	<i>FTR1</i>	High-affinity iron permease; required for mouse virulence, low-iron growth; iron, amphotericin B, caspofungin, ciclopirox, Hog1p, Sef1p, Sfu1p, and Hap43p regulated; complements <i>S. cerevisiae ftr1</i> iron transport; Hap43p repressed
CPAR2_303120	<i>CCC2</i>	Copper-transporting P-type ATPase of Golgi complex; required for wild-type iron assimilation (indirect effect via Fet3p); induced by iron starvation, ciclopirox olamine; caspofungin repressed; not required for virulence in mouse systemic infection
CPAR2_808120	<i>CFL5</i>	Ferric reductase; induced in low iron; ciclopirox olamine, flucytosine induced; amphotericin B, Sfu1 repressed; Tbf1, Hap43 induced
CPAR2_405240	<i>CCC1</i>	Manganese transporter; required for normal filamentous growth; mRNA binds She3, localized to hyphal tips; repressed by NO, alkaline pH; colony morphology-related regulation by Ssn6; regulated by Sef1, Sfu1, Hap43; Spider biofilm induced
CPAR2_402920	<i>RBT5</i>	GPI ^b -linked cell wall protein; hemoglobin utilization; Rfg1, Rim101, Tbf1, Fe regulated; Sfu1, Hog1, Tup1, serum, alkaline pH, antifungal drugs, geldamycin repressed; Hap43 induced; required for RPM1 1640 biofilms; Spider biofilm induced
CPAR2_105690	<i>HMX1</i>	Heme oxygenase; utilization of hemin iron; transcript induced by heat, low iron, or hemin; repressed by Efg1; induced by low iron; upregulated by Rim101 at pH 8; Hap43-induced; Spider and flow model biofilm induced
CPAR2_700810	<i>SFU1</i>	GATA-type transcription factor; regulator of iron-responsive genes; represses iron utilization genes if iron is present; Hap43 repressed; promotes gastrointestinal commensalism in mice; Spider biofilm induced
CPAR2_209090	<i>HAP43</i>	CCAAT-binding factor-dependent transcription factor; repressor; also called CAP2; required for low-iron response; similar to bZIP transcription factor AP-1; repressed by Sfu1; ciclopirox olamine induced; rat catheter, Spider biofilm induced
CPAR2_210100	<i>FTH1</i>	Protein similar to <i>S. cerevisiae</i> Fth1p, a high-affinity iron transporter for intravacuolar stores of iron; repressed by Sfu1p, amphotericin B, caspofungin; induced by alkaline pH, ciclopirox olamine; regulated by Sef1p, Sfu1p, and Hap43p
CPAR2_801430	<i>SEF1</i>	Zn2-Cys6 transcription factor; regulates iron uptake; negatively regulated by Sfu1p, positively regulated by Tbf1; promotes virulence in mice; mutants display decreased colonization of mouse kidneys; Spider biofilm induced
CPAR2_406510	<i>AFT2</i>	Putative Aft domain transcription factor; role in regulation of iron metabolism, oxidative stress, adhesion, hyphal growth, colony morphology, virulence; complements <i>S. cerevisiae aft1</i> mutation; Spider biofilm induced
CPAR2_407560	<i>SIT1</i>	Transporter of ferrichrome siderophores, not ferrioxamine B; required for human epithelial cell invasion in vitro, not for mouse systemic infection; regulated by iron, Sfu1, Rfg1, Tup1, Hap43; rat catheter and Spider biofilm induced
CPAR2_102830	<i>CCP1</i>	Cytochrome-c peroxidase N terminus; Rim101, alkaline pH repressed; induced in low iron or by macrophage interaction; oxygen-induced activity; regulated by Sef1, Sfu1, and Hap43; Spider biofilm induced; rat catheter biofilm repressed
CPAR2_406320	<i>HEM15</i>	Putative ferrochelatae involved in heme biosynthesis; transcript not regulated by iron levels and not affected by a yfh1 null mutation; Spider biofilm repressed

^aID, identifier.^bGPI, glycosylphosphatidylinositol.

iron-limited conditions and a reduction in hypha formation and showed a hypovirulent phenotype in a mouse model of systemic infection. Disruption of *FET33* resulted in no such defect (25, 34).

In the case of *C. parapsilosis*, our knowledge of iron homeostasis is limited. In the present study, we identified three homologues of the *S. cerevisiae* Fet3p multicopper oxidase in *C. parapsilosis* by *in silico* analysis. For further analysis, we generated a homozygous mutant strain with a deletion of the gene *CPAR2_603600* and found that the mutant strain product had 79% identity with *CaFET3* and 54% identity with *S. cerevisiae FET3* (*ScFET3*) in amino acid sequence comparison. We found that, similarly to *S. cerevisiae* and *C. albicans*, the homozygous null mutant had severe growth defects in iron-limiting medium. We can assume that, as seen with *S. cerevisiae*, the other two genes are involved in a low-affinity iron uptake system in *C. parapsilosis*, although further experiments are needed to prove this hypothesis.

In addition to playing a role in iron metabolism, fungal multicopper oxidases can play important roles in developmental processes such as fruiting body formation,

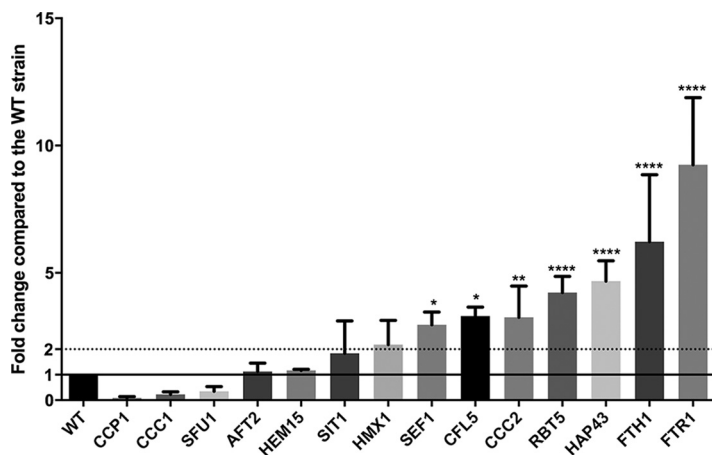


FIG 9 Expression of genes involved in iron metabolism in the homozygous deletion mutant. Expression analysis of 14 genes related to iron metabolism (GO term analysis) was performed using qPCR. The expression levels shown represent results of comparisons to the normalized wild-type (WT) values (WT value = 1; marked by line) for each gene examined. The cells were grown in YPD medium at 30°C for 4 h prior to total RNA isolation. Statistical significance was determined using one-way ANOVA coupled with Dunnett’s *post hoc* test (*, $P \leq 0.05$; **, $P \leq 0.01$; ****, $P \leq 0.0001$).

pigment formation during asexual development, pathogenesis, and competitor interactions (35). There is also a correlation between iron availability and hypha formation, and the presence of BPS induces expression of the hypha-specific *EFG1* gene in *C. albicans* (36). Deletion of *FET34* also reduces the level of hypha formation in this fungus. Although, unlike *C. albicans*, *C. parapsilosis* is unable to form true hyphae (15), different strains of *C. parapsilosis* can form pseudohyphae consisting of chain of elongated cells and morphologically distinct biofilms composed of yeast and pseudohyphae (37). The exact mechanism of the yeast-to-pseudohypha switch in *C. parapsilosis* is poorly understood. Recently, orthologues of *C. albicans* *EFG1*, *UME6*, *CPH2*, and *CZF1* were shown to play a role in morphology transition in *C. parapsilosis* (18). Among these, *CZF1* and *UME6* were also shown to be required for biofilm formation. Orthologues of *ACE2*, *BCR1*, and *EFG1* also contribute to biofilm formation in *C. parapsilosis* (38). It has also been shown previously that various metal ions influence cell differentiation during biofilm maturation in *C. albicans* and *C. tropicalis*. In *C. albicans*, both hypha formation and biofilm formation were inhibited by metallic elements such as arsenic, cadmium, chromium, cobalt, copper, selenium, silver, and zinc and enhanced by lead (39). In the

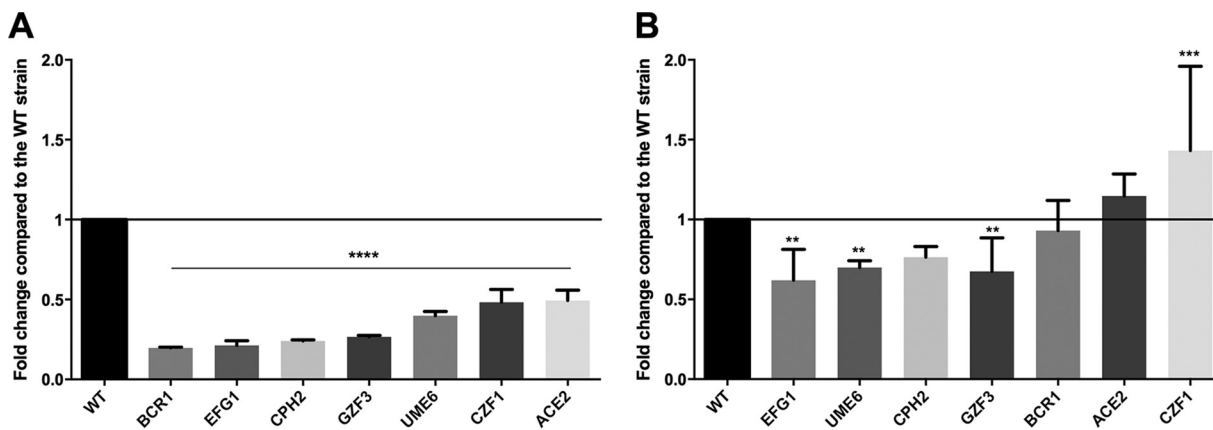


FIG 10 Expression levels of genes involved in pseudohypha and biofilm formation. Genes related to filamentous growth and biofilm formation were examined by qPCR analysis. Expression levels of the selected 7 genes were compared relative to the normalized WT values (WT value = 1). Gene expression analysis performed after growth in Spider medium at 37°C for 24 h (A) and in YPD medium at 30°C for 4 h (B). Statistical significance was determined using one-way ANOVA with Dunnett’s *post hoc* test (**, $P \leq 0.01$; ***, $P \leq 0.001$; ****, $P \leq 0.0001$).

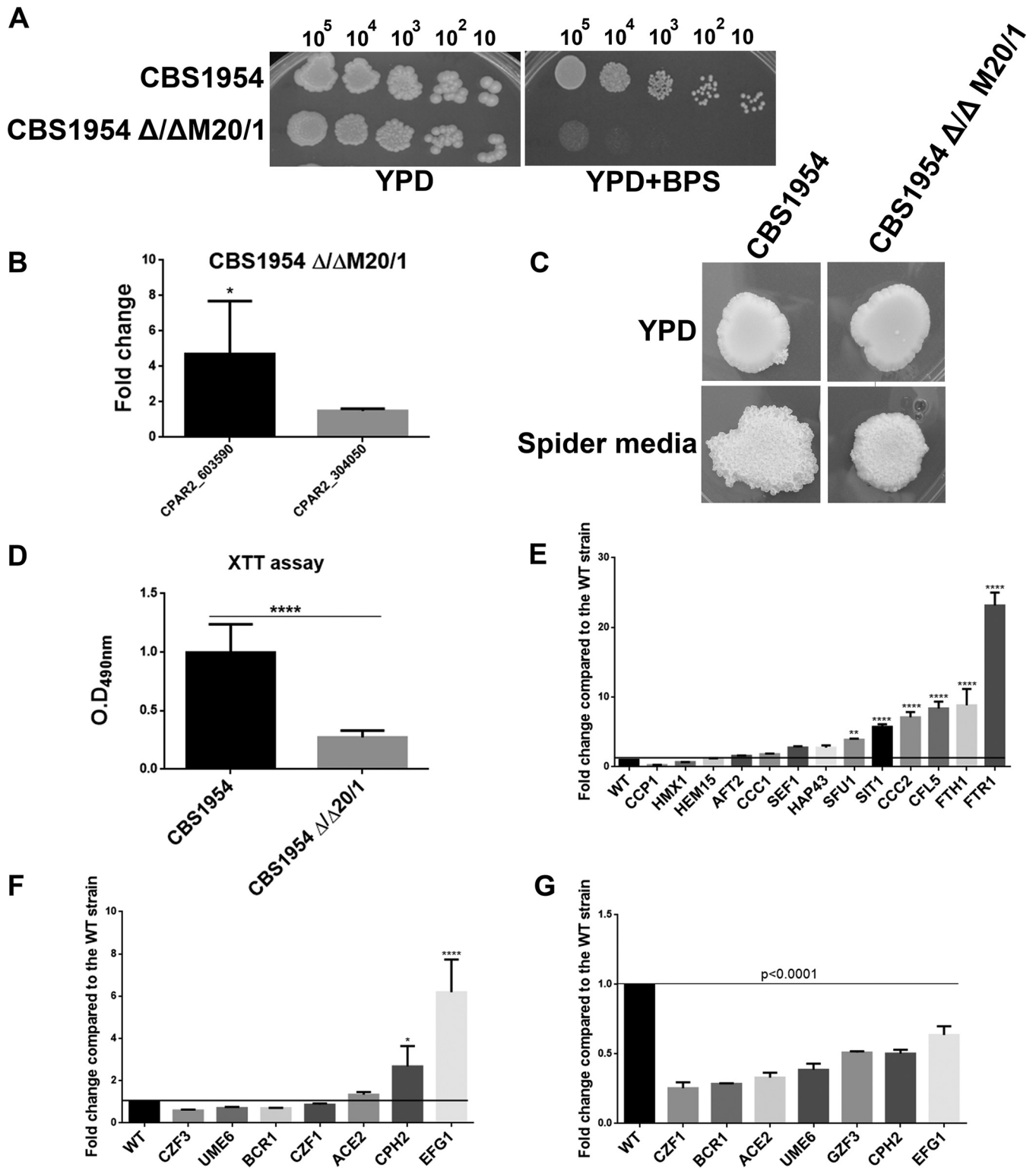


FIG 11 Characterization of *CPAR2_603600*-null mutant in CBS1954 strain. (A) Deletion mutant CBS1954 Δ/Δ M20/1 generated in environmental isolate CBS1954 showed similar growth defects under iron-restricted conditions. (B) Expression of *CPAR2_603590* and *CPAR2_304050* in the absence of *CPAR2_603600* (*, $P \leq 0.05$). (C) Decrease in filamentous growth on solid Spider medium. (D) Reduction in biofilm formation in the mutant. Statistical significance was calculated using the nonparametric *t* test (****, $P \leq 0.0001$). (E) Alteration of expression of genes involved in iron metabolism in the homozygous deletion mutant. (F) Expression of biofilm-related genes in YPD medium after growth at 30°C (*, $P \leq 0.05$; ****, $P \leq 0.0001$). (G) Expression of biofilm-related genes in Spider medium after growth at 37°C. Statistical significance was calculated using one-way ANOVA with Dunnett's *post hoc* test.

case of *C. tropicalis*, hypha formation was enhanced by chromium and zinc but inhibited by arsenic, cadmium, cobalt, copper, lead, selenium, and silver (40). Additionally, deletion of the multicopper oxidase gene *CaFET34*, but not deletion of *CaFET33*, significantly attenuated the filamentous growth of *C. albicans* (25). In the case of *C. parapsilosis*, Shafeeq et al. showed Mn^{++} -dependent biofilm formation through the activity of the biofilm regulator *BCR1* (41). All these data prompted us to investigate whether a similar effect occurs in *C. parapsilosis*. We found that the $\Delta/\Delta603600$ mutant showed a visible reduction in pseudohypha formation on solid Spider medium. Analysis of the number of pseudohyphal cells grown in liquid pseudohypha-inducing medium also showed a significant reduction in pseudohypha production. The mutant strain also showed a significant reduction in biofilm formation. But after growth in the presence of excess iron in the medium, the mutants recovered from all phenotypic defects. All the observations described above suggest that *CPAR2_603600* plays a significant role in iron metabolism and morphology transition in *C. parapsilosis*. Thus, we can assume that the proteins that are involved in morphological switching or biofilm formation in *C. parapsilosis* might require iron for their normal functioning. As we did not see a complete lack of growth of the mutant under low-iron conditions or a total absence of pseudohypha or biofilm formation, we can assume that the presence of the other two putative multicopper oxidase-encoding genes compensates for the effect of the deletion of one of the genes from the same family. Similarly to the results observed with *C. albicans*, we found that our mutant showed a significant reduction in prostaglandin production, although the $\Delta/\Delta603600$ mutant was less virulent in a mouse model of systemic infection than *C. albicans* (19). We also found that in the absence of a *FET3* homologue in *C. parapsilosis*, several homologues of iron metabolism genes showed higher expression, which can also be a counteracting phenomenon operating to reduce the defect of the lack of a high-affinity iron oxidase in *C. parapsilosis*. Taken together, our data give a novel insight into the role of a multicopper oxidase gene in iron homeostasis maintenance, morphology, and biofilm regulation in the human-pathogenic fungus *C. parapsilosis*. However, further investigation is needed to understand the complete mechanism of iron metabolism in this emerging pathogen.

MATERIALS AND METHODS

Strains. All *C. parapsilosis* strains used in this study are listed in Table S1 in the supplemental material.

Primers. All the primers used in this study are listed in Table S2. Descriptions of the real-time primers for genes involved in pseudohypha and biofilm formation are available in our previous publication (18).

Media and growth conditions. All *C. parapsilosis* strains were cultivated in YPD (1% dextrose, 1% peptone, and 0.5% yeast extract) at 30°C. Transformants containing the *LEU2* and *HIS1* markers were maintained on Synthetic Complete medium (SC; 2% dextrose, 0.95% yeast nitrogen base, mixture of amino acids, 2% agar) without leucine and histidine. Nourseothricin-resistant colonies were maintained on YPD plates supplemented with 100 $\mu\text{g}/\text{ml}$ nourseothricin.

Construction of deletion mutant strains. Deletion of *CPAR_603600* was performed with the fusion PCR method as described in our previous publication (19). For gene deletion in an environmental isolate of *C. parapsilosis* (CBS1954 strain), the pSF52SaFET3 plasmid was used. Disruption of the 1,884-bp open reading frame (ORF) was performed as described previously by Horvath et al. (42).

Gene reintegration. The DNA construct for reintegration was generated with fusion PCR. The first (2,875-bp) fragment was amplified using the primer pair UpFP and ORF-UP-RP-Fus (see file S2 in the supplemental material) and consisted of 1,000 bp upstream of the ORF and the ORF without the stop codon. The second (3,151-bp) mCherry-NAT fragment was amplified using mCherry-FP-Fus and mCherry-RP-Fus with pMG2343 plasmid (43) as the template. The third and final (948-bp) downstream fragment was amplified using the primer pair ORF-DN-Fp-Fus and ORF-DN-RP. After purification of all the three fragments, fusion PCR was performed to join all three fragments to generate the final 6,974-bp DNA construct. After gel purification, this DNA construct was used to transform the $\Delta/\Delta603600$ 2/1 strain and the transformants were selected on a YPD plate containing 100 $\mu\text{g}/\text{ml}$ nourseothricin. The transformants were confirmed by Southern blotting, and expression of the gene was also verified by qRT-PCR analysis.

Phenotypic characterization. Growth of the mutant strains was examined under various conditions, designed to identify nutritional, cell wall, and osmotic- and oxidative-stressor-responsive phenotypes (18). All deletion mutant strains were grown in 2 ml of YPD medium prior to each experiment at 30°C overnight. The cultures were then washed three times with 1× phosphate-buffered saline (PBS) and diluted in 1× PBS after the desired cell concentrations were determined. A 5- μl volume from each dilution was plated on various plates followed by incubation for 2 to 3 days at 30°C.

Pseudohypha formation on solid plates. After the desired cell concentration (optical density [OD] of 0.08) was set, cells were plated on YPD medium and pseudohypha-inducing Spider medium (1% peptone, 1% yeast extract, 1% mannitol, 0.5% NaCl, 0.2% K_2HPO_4) (44) and incubated at 37°C for 7 days.

Morphology analysis by fluorescence-activated cell sorter (FACS) analysis. Cells were collected from overnight cultures (37°C, 5% CO_2) from YPD and Spider media and suspended in 1 ml of 4% paraformaldehyde followed by 30 min of incubation at room temperature, with continuous rotation. Following incubation, cells were washed four times with 1× PBS, and pellets were suspended in 0.5 ml 1% bovine serum albumin (BSA) (Sigma-Aldrich), followed by incubation at room temperature for additional 30 min with rotation. The cells were then washed three times with 1× PBS and suspended in 200 to 400 μ l of the same buffer, depending on the cell concentration (approximately 10^8 /ml cell). Then, 100 μ l of the suspension was transferred into a new Eppendorf tube and the morphology was analyzed by the use of Amnis Flowsight and the pseudohyphae were quantified by the use of IDEAS software (Amnis).

Biofilm formation. Biofilm formation was examined in liquid Spider medium by analysis of growth in 96-well polystyrene plates. All *C. parapsilosis* strains were grown overnight in YPD at 30°C and were then diluted to an optical density at 600 nm (OD_{600}) of 0.5 in 2 ml of Spider medium. The 96-well flat bottom microtiter plates were pretreated overnight with 10% FBS and then washed 2 times with 1× PBS before addition of 100 μ l of cell suspension (5×10^5 cells) from the Spider medium. Cells were incubated at 37°C for 90 min at 180 rpm for initial adherence of the biofilm. The wells were then washed 2 times with 1× PBS, and 100 μ l of fresh Spider medium was added to each well. The plates were kept at 37°C for 48 h before the quantification.

XTT reduction assay. Biofilm formation was quantified using the XTT reduction assay (45). Briefly, 0.5 mg/ml XTT solution in PBS was prepared, filter sterilized, and stored at -70°C. Menadione solution (10 mM) in acetone was prepared freshly immediately before use. Prior to the assay, 1 μ l of menadione solution was added to 10 ml of PBS. First, the biofilms were washed 3 times with 1× PBS and then 200 μ l of XTT-menadione solution (ratio of 5 to 1 by volume) was added to each well. The plate was then incubated at 37°C for 2 h in the dark. After incubation, 100 μ l of each solution was transferred to another 96-well plate and measured with a microtiter plate reader at 490 nm. Ten technical parallels were used per strain, and cell-free Spider medium was used as a control. The values of the control wells were subtracted from the test absorbance values to reduce the background interference. Three independent experiments were performed for the assay.

RNA extraction and reverse transcription-PCR. For RNA extraction, all *C. parapsilosis* strains were grown overnight in 2 ml of YPD medium at 30°C with shaking applied at 180 rpm. The next day, the cells were freshly inoculated in 5 ml of YPD or YPD supplemented with 100 μ M/ml BPS (OD of 0.2). For gene expression analysis, strains were grown overnight in 2 ml YPD medium at 30°C with shaking applied at 180 rpm, followed by washing steps performed with 1× PBS, and were reinoculated in liquid Spider medium for incubation at 37°C for 24 h. RNA was isolated using a RiboPure yeast RNA isolation kit (Ambion) following the manufacturer's instruction. A total of 500 ng RNA was used for cDNA synthesis. cDNA was synthesized using a RevertAid First Strand cDNA synthesis kit (Thermo Scientific) according to the manufacturer's instruction.

Real-time PCR. Real-time PCR was carried out in a final volume of 20 μ l using Maxima SYBR green/fluorescein qPCR Master Mix (Thermo Scientific) (2×). The reaction was performed in a C1000 thermal cycler (Bio-Rad) using the following reaction conditions: 95°C for 3 min, 95°C for 10 s, 60°C for 30 s, and 65°C for 5 s for 50 cycles. Fold change in mRNA expression was calculated by the threshold cycle ($\Delta\Delta C_T$) method (real-time PCR applications guide; Bio-Rad). *TUB4* was used as a housekeeping gene as an internal control.

Statistical analysis. One-way analysis of variance (ANOVA) was used to determine the differences in biofilm formation by different strains. Differences were considered statistically significant at *P* values of ≤ 0.05 (*, $P \leq 0.05$; **, $P \leq 0.01$; ***, $P \leq 0.001$; ****, $P \leq 0.0001$).

SUPPLEMENTAL MATERIAL

Supplemental material is available online only.

FIG S1, TIF file, 0.5 MB.

FIG S2, TIF file, 1.4 MB.

FIG S3, TIF file, 1.3 MB.

FIG S4, JPG file, 2.2 MB.

TABLE S1, XLSX file, 0.01 MB.

TABLE S2, DOCX file, 0.02 MB.

ACKNOWLEDGMENTS

We thank Judith Berman for providing us with mCherry plasmid. We thank Csaba Papp and Attila Farkas for assisting with the scanning electron microscopy. We are also thankful to Joshua D. Nosanchuk for critically reading the manuscript and giving valuable suggestions.

T.C. was supported by the European Union Seventh Framework Program (FP7/2007-2013) under grant agreements FP7-PEOPLE-2013-ITN-606786 (ImResFun). Z.T. was sup-

ported by the Szeged Scientists Academy under the sponsorship of the Hungarian Ministry of Human Capacities (EMMI:11136-2/2019/FIRFIN). A.G. was supported by grants 20391 3/2018/FEKUSTRAT, NKFIH K 123952, and GINOP-2.3.2.-15-2016-00035. A.G. was additionally funded by LP2018-15/2018.

We declare that the research was conducted in the absence of any commercial or financial relationships that could be construed as a potential conflict of interest.

REFERENCES

- Haas H, Eisendle M, Turgeon BG. 2008. Siderophores in fungal physiology and virulence. *Annu Rev Phytopathol* 46:149–187. <https://doi.org/10.1146/annurev.phyto.45.062806.094338>.
- Halliwell B, Gutteridge JM. 1984. Oxygen toxicity, oxygen radicals, transition metals and disease. *Biochem J* 219:1–14. <https://doi.org/10.1042/bj2190001>.
- De Silva DM, Askwith CC, Eide D, Kaplan J. 1995. The FET3 gene product required for high affinity iron transport in yeast is a cell surface ferroxidase. *J Biol Chem* 270:1098–1101. <https://doi.org/10.1074/jbc.270.3.1098>.
- Yamaguchi-Iwai Y, Dancis A, Klausner RD. 1995. AFT1: a mediator of iron regulated transcriptional control in *Saccharomyces cerevisiae*. *EMBO J* 14:1231–1239. <https://doi.org/10.1002/j.1460-2075.1995.tb07106.x>.
- Askwith C, Eide D, Van Ho A, Bernard PS, Li L, Davis-Kaplan S, Sipe DM, Kaplan J. 1994. The FET3 gene of *S. cerevisiae* encodes a multicopper oxidase required for ferrous iron uptake. *Cell* 76:403–410. [https://doi.org/10.1016/0092-8674\(94\)90346-8](https://doi.org/10.1016/0092-8674(94)90346-8).
- Ding C, Festa RA, Sun T-S, Wang Z-Y. 2014. Iron and copper as virulence modulators in human fungal pathogens. *Mol Microbiol* 93:10–23. <https://doi.org/10.1111/mmi.12653>.
- Gerwien F, Skrahina V, Kasper L, Hube B, Brunke S. 1 January 2018, posting date. Metals in fungal virulence. *FEMS Microbiol Rev* <https://doi.org/10.1093/femsre/fux050>.
- Almeida RS, Wilson D, Hube B. 2009. *Candida albicans* iron acquisition within the host. *FEMS Yeast Res* 9:1000–1012. <https://doi.org/10.1111/j.1567-1364.2009.00570.x>.
- Noble SM. 2013. *Candida albicans* specializations for iron homeostasis: from commensalism to virulence. *Curr Opin Microbiol* 16:708–715. <https://doi.org/10.1016/j.mib.2013.09.006>.
- Gerwien F, Safyan A, Wisgott S, Hille F, Kaemmer P, Linde JJ, Brunke S, Kasper L, Hube B. 2016. A novel hybrid iron regulation network combines features from pathogenic and nonpathogenic yeasts. *mBio* 7:e01782-16. <https://doi.org/10.1128/mBio.01782-16>.
- Gerwien F, Safyan A, Wisgott S, Brunke S, Kasper L, Hube B. 2017. The fungal pathogen *Candida glabrata* does not depend on surface ferric reductases for iron acquisition. *Front Microbiol* 8:1055. <https://doi.org/10.3389/fmicb.2017.01055>.
- Eck R, Hundt S, Härtl A, Roemer E, Künkel W. 1999. A multicopper oxidase gene from *Candida albicans*: cloning, characterization and disruption. *Microbiology* 145:2415–2422. <https://doi.org/10.1099/00221287-145-9-2415>.
- Chen C, Pande K, French SD, Tuch BB, Noble SM. 2011. An iron homeostasis regulatory circuit with reciprocal roles in *Candida albicans* commensalism and pathogenesis. *Cell Host Microbe* 10:118–135. <https://doi.org/10.1016/j.chom.2011.07.005>.
- Pammi M, Holland L, Butler G, Gacser A, Bliss JM. 2013. *Candida parapsilosis* is a significant neonatal pathogen: a systematic review and meta-analysis. *Pediatr Infect Dis J* 32:e206–16. <https://doi.org/10.1097/INF.0b013e3182863a1c>.
- Trofa D, Gacser A, Nosanchuk JD. 2008. *Candida parapsilosis*, an emerging fungal pathogen. *Clin Microbiol Rev* 21:606–625. <https://doi.org/10.1128/CMR.00013-08>.
- Kuhn DM, Mukherjee PK, Clark TA, Pujol C, Chandra J, Hajjeh RA, Warnock DW, Soll DR, Ghannoum MA. 2004. *Candida parapsilosis* characterization in an outbreak setting. *Emerg Infect Dis* 10:1074–1081. <https://doi.org/10.3201/eid1006.030873>.
- Toth R, Nosek J, Mora-Montes HM, Gabaldon T, Bliss JM, Nosanchuk JD, Turner SA, Butler G, Vagvolgyi C, Gacser A. 27 February 2019, posting date. *Candida parapsilosis*: from genes to the bedside. *Clin Microbiol Rev* <https://doi.org/10.1128/CMR.00111-18>.
- Tóth R, Cabral V, Thuer E, Bohner F, Németh T, Papp C, Nimrichter L, Molnár G, Vágvolgyi C, Gabaldón T, Nosanchuk JD, Gácsér A. 2018. Investigation of *Candida parapsilosis* virulence regulatory factors during host-pathogen interaction. *Sci Rep* 8:1346. <https://doi.org/10.1038/s41598-018-19453-4>.
- Chakraborty T, Thuer E, Heijink M, Toth R, Bodai L, Vagvolgyi C, Giera M, Gabaldon T, Gacser A. 2018. Eicosanoid biosynthesis influences the virulence of *Candida parapsilosis*. *Virulence* 9:1019–1035. <https://doi.org/10.1080/21505594.2018.1475797>.
- Skrzypek MS, Binkley J, Binkley G, Miyasato SR, Simison M, Sherlock G. 2017. The *Candida* Genome Database (CGD): incorporation of assembly 22, systematic identifiers and visualization of high throughput sequencing data. *Nucleic Acids Res* 45:D592–D596. <https://doi.org/10.1093/nar/gkw924>.
- Madeira F, Park YM, Lee J, Buso N, Gur T, Madhusoodanan N, Basutkar P, Tivey ARN, Potter SC, Finn RD, Lopez R. 2019. The EMBL-EBI search and sequence analysis tools APIs in 2019. *Nucleic Acids Res* 47:W636–W641. <https://doi.org/10.1093/nar/gkz268>.
- Robert X, Gouet P. 2014. Deciphering key features in protein structures with the new ENDscript server. *Nucleic Acids Res* 42:W320–W324. <https://doi.org/10.1093/nar/gku316>.
- Pryszcz LP, Nemeth T, Gacser A, Gabaldon T. 2013. Unexpected genomic variability in clinical and environmental strains of the pathogenic yeast *Candida parapsilosis*. *Genome Biol Evol* 5:2382–2392. <https://doi.org/10.1093/gbe/evt185>.
- Holland LM, Schroder MS, Turner SA, Taff H, Andes D, Grozer Z, Gacser A, Ames L, Haynes K, Higgins DG, Butler G. 2014. Comparative phenotypic analysis of the major fungal pathogens *Candida parapsilosis* and *Candida albicans*. *PLoS Pathog* 10:e1004365. <https://doi.org/10.1371/journal.ppat.1004365>.
- Cheng X, Xu N, Yu Q, Ding X, Qian K, Zhao Q, Wang Y, Zhang B, Xing L, Li M. 2013. Novel insight into the expression and function of the multicopper oxidases in *Candida albicans*. *Microbiology* 159:1044–1055. <https://doi.org/10.1099/mic.0.065268-0>.
- Lan CY, Rodarte G, Murillo LA, Jones T, Davis RW, Dungan J, Newport G, Agabian N. 2004. Regulatory networks affected by iron availability in *Candida albicans*. *Mol Microbiol* 53:1451–1469. <https://doi.org/10.1111/j.1365-2958.2004.04214.x>.
- Reuss O, Vik A, Kolter R, Morschhauser J. 2004. The SAT1 flipper, an optimized tool for gene disruption in *Candida albicans*. *Gene* 341:119–127. <https://doi.org/10.1016/j.gene.2004.06.021>.
- Hammacott JE, Williams PH, Cashmore AM. 2000. *Candida albicans* CFL1 encodes a functional ferric reductase activity that can rescue a *Saccharomyces cerevisiae* fre1 mutant. *Microbiology* 146:869–876. <https://doi.org/10.1099/00221287-146-4-869>.
- Knight SAB, Dancis A. 2006. Reduction of 2,3-bis(2-methoxy-4-nitro-5-sulfophenyl)-2H-tetrazolium-5-carboxanilide inner salt (XTT) is dependent on CaFRE10 ferric reductase for *Candida albicans* grown in unbuffered media. *Microbiology* 152:2301–2308. <https://doi.org/10.1099/mic.0.28843-0>.
- Knight SAB, Vilaire G, Lesuisse E, Dancis A. 2005. Iron acquisition from transferrin by *Candida albicans* depends on the reductive pathway. *Infect Immun* 73:5482–5492. <https://doi.org/10.1128/IAI.73.9.5482-5492.2005>.
- Knight SAB, Lesuisse E, Stearman R, Klausner RD, Dancis A. 2002. Reductive iron uptake by *Candida albicans*: role of copper, iron and the TUP1 regulator. *Microbiology* 148:29–40. <https://doi.org/10.1099/00221287-148-1-29>.
- Ramanan N, Wang Y. 2000. A high-affinity iron permease essential for *Candida albicans* virulence. *Science* 288:1062–1064. <https://doi.org/10.1126/science.288.5468.1062>.
- Erb-Downward JR, Noverr MC. 2007. Characterization of prostaglandin E2 production by *Candida albicans*. *Infect Immun* 75:3498–3505. <https://doi.org/10.1128/IAI.00232-07>.
- Mamouei Z, Zeng G, Wang YY-M, Wang YY-M. 2017. *Candida albicans* possess a highly versatile and dynamic high-affinity iron transport sys-

- tem important for its commensal-pathogenic lifestyle. *Mol Microbiol* 106:986–998. <https://doi.org/10.1111/mmi.13864>.
35. Hoegger PJ, Kilaru S, James TY, Thacker JR, Kues U. 2006. Phylogenetic comparison and classification of laccase and related multicopper oxidase protein sequences. *FEBS J* 273:2308–2326. <https://doi.org/10.1111/j.1742-4658.2006.05247.x>.
 36. Hameed S, Prasad T, Banerjee D, Chandra A, Mukhopadhyay CK, Goswami SK, Lattif AA, Chandra J, Mukherjee PK, Ghannoum MA, Prasad R. 2008. Iron deprivation induces EFG1-mediated hyphal development in *Candida albicans* without affecting biofilm formation. *FEMS Yeast Res* 8:744–755. <https://doi.org/10.1111/j.1567-1364.2008.00394.x>.
 37. Pannanusorn S, Ramírez-Zavala B, Lünsdorf H, Agerberth B, Morschhäuser J, Römling U. 2014. Characterization of biofilm formation and the role of BCR1 in clinical isolates of *Candida parapsilosis*. *Eukaryot Cell* 13:438–451. <https://doi.org/10.1128/EC.00181-13>.
 38. Ding C, Butler G. 2007. Development of a gene knockout system in *Candida parapsilosis* reveals a conserved role for BCR1 in biofilm formation. *Eukaryot Cell* 6:1310–1319. <https://doi.org/10.1128/EC.00136-07>.
 39. Harrison JJ, Ceri H, Yerly J, Rabiei M, Hu Y, Martinuzzi R, Turner RJ. 2007. Metal ions may suppress or enhance cellular differentiation in *Candida albicans* and *Candida tropicalis* biofilms. *Appl Environ Microbiol* 73:4940–4949. <https://doi.org/10.1128/AEM.02711-06>.
 40. Odds FC. 1988. *Candida and candidosis: a review and bibliography*. Baillière Tindall, Kent, United Kingdom.
 41. Shafeeq S, Pannanusorn S, Elsharabasy Y, Ramírez-Zavala B, Morschhäuser J, Römling U. 1 September 2019, posting date. Impact of manganese on biofilm formation and cell morphology of *Candida parapsilosis* clinical isolates with different biofilm forming abilities. *FEMS Yeast Res* <https://doi.org/10.1093/femsyr/foz057>.
 42. Horvath P, Nosanchuk JD, Hamari Z, Vagvolgyi C, Gacsér A. 2012. The identification of gene duplication and the role of secreted aspartyl proteinase 1 in *Candida parapsilosis* virulence. *J Infect Dis* 205:923–933. <https://doi.org/10.1093/infdis/jir873>.
 43. Gerami-Nejad M, Forche A, McClellan M, Berman J. 2012. Analysis of protein function in clinical *C. albicans* isolates. *Yeast* 29:303–309. <https://doi.org/10.1002/yea.2910>.
 44. Liu H, Kohler J, Fink GR. 1994. Suppression of hyphal formation in *Candida albicans* by mutation of a STE12 homolog. *Science* 266:1723–1726. <https://doi.org/10.1126/science.7992058>.
 45. Jin Y, Yip HK, Samaranayake YH, Yau JY, Samaranayake LP. 2003. Biofilm-forming ability of *Candida albicans* is unlikely to contribute to high levels of oral yeast carriage in cases of human immunodeficiency virus infection. *J Clin Microbiol* 41:2961–2967. <https://doi.org/10.1128/JCM.41.7.2961-2967.2003>.